Simulation of near-field scanning optical microscopy using a plasmonic gap probe

Kazuo Tanaka and Masahiro Tanaka

Department of Electronics and Computer Engineering, Gifu University, Yanagido 1-1, Gifu City, Japan 501-1193
tanaka@tnk.info.gifu-u.ac.jp

Kiyofumi Katayama

Faculty of Administration and Informatics, University of Hamamatsu, Hamamatsu City, Japan 431-2102

Abstract: Imaging by near-field scanning optical microscopy (NSOM) with a plasmonic gap probe (PGP) is simulated to confirm the operation of the recently proposed PGP. The simulations demonstrate that the probe works in illumination, collection-reflection and collection mode, and that is it not necessary to vibrate the probe tip in order to remove background noise. The resolution of the scanned image is also shown to be approximately equal to the diameter of the probe tip. Furthermore, the throughput of the probe is much higher than conventional aperture probes providing similar resolution. The proposed probe thus has the advantages of both aperture probes and scattering probes, and is expected to have excellent characteristics for use as a scanning probe for NSOM.

OCIS codes: (180.5810) Scanning microscopy; (240.6680) Surface plasmons

References and links

1. K. Tanaka, M. Tanaka, and T. Sugiyama, "Metallic tip-probe providing high intensity and small spot size with a small background light in near-field optics," Appl. Phys. Lett. **87**, 151116 (2005).
2. K. Tanaka, M. Tanaka, and T. Sugiyama, "Creation of strongly localized and strongly enhanced optical near-field on metallic probe-tip with surface plasmon polaritons," Opt. Express **14**, 832-846 (2006).
3. C. Girard, A. Dereux, and O. J. F. Martin, "Importance of confined fields in near-field optical imaging of subwavelength objects," Phys. Rev. B **50**, 14467-14473 (1994).
4. M. Xiao, "Theoretical treatment for scattering scanning near-field optical microscopy," J. Opt. Soc. Am. A **14**, 2977-2984 (1997).
5. S. I. Bozhevolnyi, M. Xiao, and J. M. Hvan, "Polarization-resolved imaging with a reflection near-field optical microscope," J. Opt. Soc. Am. A **16**, 2649-2657 (1999).
6. T. Setala, M. Kaivola, and A. T. Friberg, "Evanescent and propagating electromagnetic fields in scattering from point-dipole structure," J. Opt. Soc. Am. A **18**, 678-688 (2001).
7. K. Tanaka, M. Yan, and M. Tanaka, "A simulation of near field optics by three dimensional volume integral equation of classical electromagnetic theory," Opt. Rev. **8**, 43-53 (2001).
8. G. von Freymann, T. Schimmel, and M. Wegener, "Computer simulations on near-field scanning optical microscopy: Can subwavelength resolution be obtained using uncoated optical fiber probe?" Appl. Phys. Lett. **73**, 1170-1172 (1998).
9. Y. Sasaki and H. Sasaki, "Probe design optimization for a high-resolution scattering-type scanning near-field optical microscope," J. Microscopy **202**, 347-350 (2001).
10. K. Tanaka and M. Tanaka, "Simulation of an aperture in the thick metallic screen that gives high intensity and small spot size using surface plasmon polariton," J. Microscopy **210**, 294-300 (2003).
11. K. Tanaka and M. Tanaka, "Optimized computer-aided design of I-shaped subwavelength aperture for high intensity and small spot size," Opt. Comm. **233**, 231-244 (2004).
12. P. Zwamborn and P. M. van den Berg, "The three-dimensional weak form of the conjugate gradient FFT method for solving scattering problems," IEEE Trans. Microwave Theory Tech. **40**, 1757-1766 (1992).

#72603 - $15.00 USD Received 5 July 2006; revised 25 September 2006; accepted 30 September 2006

13. R. Barrett, T. Berry, T. F. Chan, J. Demmel, J. Donato, J. Dongarra, V. Eijkhout, R. Pozo, C. Romine, and H. van der Vorst, *Templates for the Solution of Linear Systems: Building Blocks for Iterative Methods*, (Society for Industrial and Applied Mathematics, New York, 1994).
14. E. K. Miller, L. Medgyesi-Mitschnag, and E. H. Newsman, ed., *Computational Electromagnetics Frequency-Domain Method of Moments*, (The Institute of Electrical and Electronics Engineers, 1992).
15. G. S. Smith, *An introduction to classical electromagnetic radiation* (Cambridge Uni. Press, 1997).
16. M. Ohtsu, ed., *Near-field Nano/Atom Optics and Technology*, (Springer-Verlag, Tokyo, 1998), Chap. 4.
17. S. Kawata, M. Ohtsu, and M. Irie, eds., *Nano-Optics*, (Springer- Verlag, Berlin Heidelberg, 2002), Chap. 5.
18. J. A. Veerman, A. M. Otter, L. Kuipers, and N. F. van Hulst, "High definition aperture probes for near-field optical microscopy fabricated by focused ion beam milling," Appl. Phys. Lett. **72**, 3115-3117 (1998).
19. M. Ohtsu, ed., *Near-field Nano/Atom Optics and Technology*, (Springer-Verlag, Tokyo, 1998) Chap. 2.
20. F. Zenhausern, Y. Martin, and H. K. Wickramasinghe, "Scanning interferometric apertureless microscopy: Optical imaging at 10 angstrom resolution," Science **269**, 1083-1085 (1995).
21. Y. Inoue and S. Kawata, "A scanning near-field optical microscope having scanning electron tunneling microscope capability using a single metallic probe tip," J. Microscopy **178**, 14-19 (1994).
22. J. M. Gerton, L. A. Wade, G. A. Lessard, Z. Ma, and S. R. Quake, "Tip-enhanced fluorescent microscopy at 10 nanometer resolution," Phys. Rev. Lett. **93**, 18080 (2004).

1. Introduction

The present authors recently proposed an interesting metallic aperture probe that reveals strongly localized and strongly enhanced near fields at the probe tip via the surface plasmon polariton (SPP), called the plasmonic gap probe (PGP) [1, 2]. In application of the proposed PGP as a scanning probe for near-field scanning optical microscopy (NSOM), the resolution will be determined by the tip radius, since the optical near field is strongly localized at the PGP probe tip. As the optical near field at the probe tip is created by the wave transmitted through the aperture, direct illumination of the probe tip by an external light source is not necessary. This technique is therefore expected to offer low background noise, rendering it no longer necessary to vibrate the probe tip in order to remove background noise. The proposed PGP is used as an aperture probe, and it is possible to create the structure on the tip of an optical fiber. The PGP is thus expected to offer the advantages of both aperture probes and scattering probes.

In this paper, three-dimensional (3D) imaging simulations of NSOM using the PGP are presented as an example of the performance of the PGP under practical conditions. Simulations of imaging for a nanometric dielectric object demonstrate that the PGP functions as expected in illumination mode, collection-reflection mode, and collection mode with resolution approximately correspondent to the tip diameter of the probe.

A number of 3D imaging simulations for NSOM using aperture and scattering probes under practical conditions have been reported [3-7]. However, most simulations examining the relationship between resolution and tip radius in NSOM using a scattering probe have been performed on the assumption that the probe tip is approximated by a small and isolated spherical object with radius equal to the tip radius. However, under practical conditions, incident light is scattered not just by the tip, and the additional scatter degrades the resolution [8, 9]. Imaging simulations of NSOM under practical condition without the assumption of a simple spherical probe tip thus remain important. The present simulations were conducted without such an assumption in order to determine the characteristics and performance of the PGP under practical conditions.

2. Plasmonic gap probe consisting of I-shaped aperture and pyramidal structure

The schematic model of the NSOM system equipped with the PGP is shown in Fig. 1. A uniform metallic screen with thickness w and relative complex-valued permittivity ε_1 is placed on the x-y plane. A pyramidal structure of the same metal is fabricated on this screen, and an

#72603 - $15.00 USD Received 5 July 2006; revised 25 September 2006; accepted 30 September 2006

I-shaped aperture consisting of a rectangular narrow gap-region of $a_x \times a_y$ sandwiched by two rectangular wide gap-regions of $b_x \times b_y$ is formed in the screen through the pyramidal structure. The pyramidal structure is divided into two sections by the long I-shaped aperture. The height from the screen to the tip of the left section is assumed to be greater than the height from the screen to the tip of the right section, and the left section is used as a tapered metallic probe. The base of the pyramidal structure has dimensions of $B_x \times B_y$. For simplicity, $B_y = 2b_y + a_y = B_x$ is assumed. A Gaussian beam is set normally incident to the screen from the negative z direction below the metallic screen in region (I), and the electric field polarization at $z = 0$ is set parallel to the x axis. The SSPs exiting the I-shaped aperture from the incident beam are confined and enhanced in the narrow gap region in the aperture [10, 11]. The SPPs propagate along the narrow gap region through the pyramidal structure and along the side boundary of the left section. Finally, the SPPs reach the tip of the left section shown in Fig. 1 and are focused at the sharp small-radius tip. It has been shown that a near field with high intensity and small spot size can be created near the tip of the probe [2].

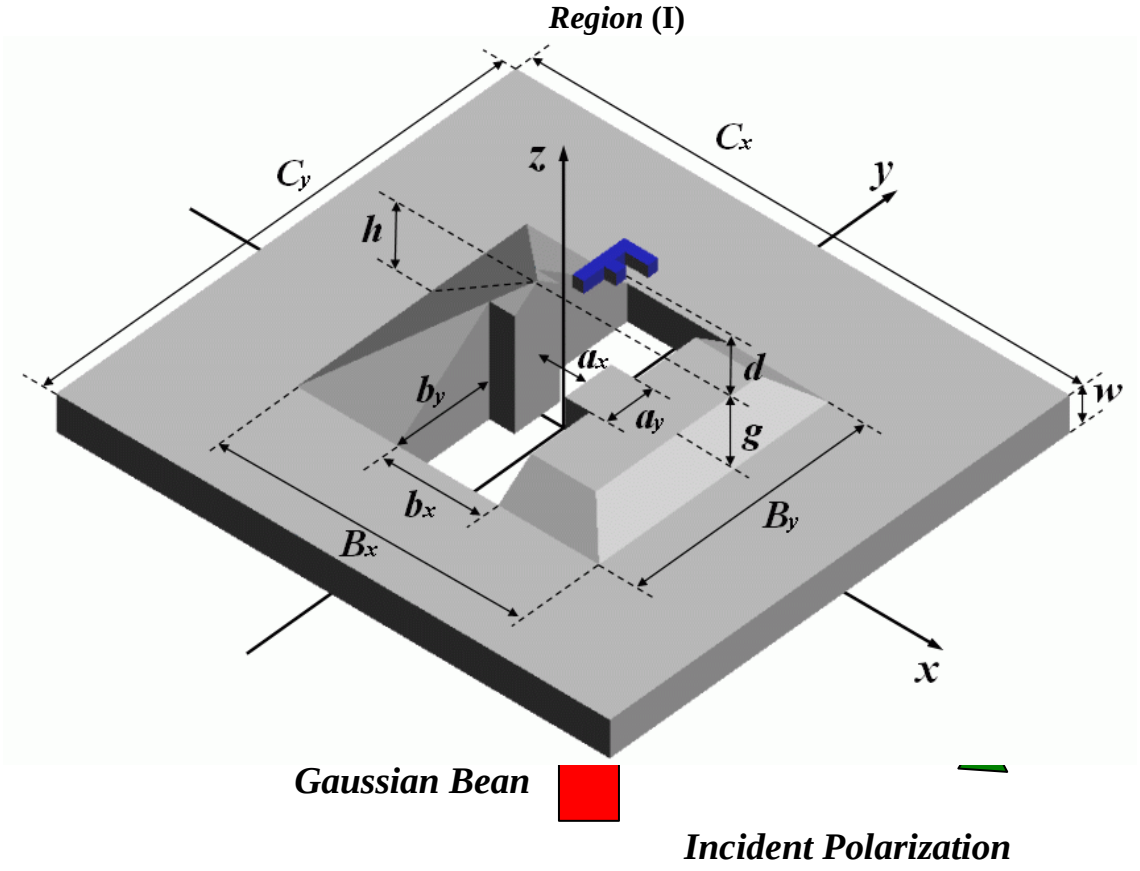

Fig. 1. Geometry of image formation by NSOM with PGP. The dielectric F-shaped object (blue) is illuminated by the near field created by the probe tip and scanned in the x and y directions with respect to the probe. The incident wave is assumed to be Gaussian beam.

The object to be scanned in the simulation is a nanometric and planar F-shaped dielectric object consisting of eight unit cubes with side length δ (Fig. 2). The object is set on a plane parallel to the x-y plane (Fig. 2). The probe scans two-dimensionally on the object plane under the condition that the distance d between the probe tip and the object plane is maintained

#72603 - $15.00 USD Received 5 July 2006; revised 25 September 2006; accepted 30 September 2006

constant (Fig. 1). The scattered power is calculated in the upper region (I) and lower region (II) of the screen, and is regarded as the signal of the dielectric object observed by the NSOM. The simulated image is created once the dependence of the signal on the position of the probe tip has been determined.

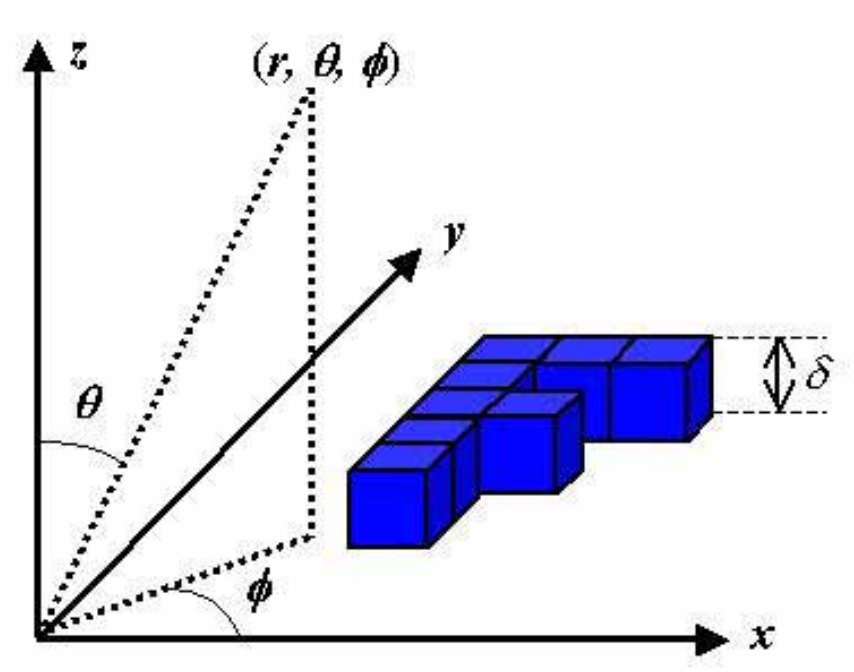

Fig. 2. Nanometric 3D dielectric F-shaped object on the plane parallel to the *x*-*y* plane. The dielectric F-shaped object consists of eight equal-sized cubes with side length δ.

3. Volume integral equation

The scattering problem for the NSOM structure shown in Fig. 1 is solved using a volume integral equation (VIE) under the assumption of exp(*j*ω*t*) time dependence [12], as given by

$$\boldsymbol{E}^{i}(\boldsymbol{x}) = \boldsymbol{D}(\boldsymbol{x})/\varepsilon_{\mathrm{r}}(\boldsymbol{x}) - (k_0^2 + \nabla\nabla\bullet)\boldsymbol{A}(\boldsymbol{x}) \tag{1}$$

Here, $\boldsymbol{D}(\boldsymbol{x})$ is the total electric flux, $\boldsymbol{E}^{\mathrm{i}}(\boldsymbol{x})$ is the incident electric field vector, $k_0 = \omega/c$, where c is the velocity of light in free space and ω is angular frequency, and $\boldsymbol{A}(\boldsymbol{x})$ is the vector potential, which is expressed by the following volume integral.

$$\boldsymbol{A}(\boldsymbol{x}) = (1/\varepsilon_0)\iiint_V [(\varepsilon_{\mathrm{r}}(\boldsymbol{x}') - \varepsilon_0)/\varepsilon_{\mathrm{r}}(\boldsymbol{x}')]G(\boldsymbol{x}|\boldsymbol{x}')\boldsymbol{D}(\boldsymbol{x}')\mathrm{d}v' \tag{2}$$

Here, $G(\boldsymbol{x}|\boldsymbol{x}')$ is a three-dimensional free-space Green's function given by

$$G(\boldsymbol{x}|\boldsymbol{x}') = \exp(-jk_0|\boldsymbol{x} - \boldsymbol{x}'|)/(4\pi|\boldsymbol{x} - \boldsymbol{x}'|) \tag{3}$$

The volume integral region V in Eq. (2) represents the entire space, and $\varepsilon_{\mathrm{r}}(\boldsymbol{x})$ represents the distribution of relative permittivity, where $\varepsilon_{\mathrm{r}}(\boldsymbol{x})/\varepsilon_0 = \varepsilon_1$ for the metal of the screen, $\varepsilon_{\mathrm{r}}(\boldsymbol{x})/\varepsilon_0 = \varepsilon_2$ for the dielectric object, and $\varepsilon_{\mathrm{r}}(\boldsymbol{x})/\varepsilon_0 = 1$ for the aperture and free space. To obtain the solution, the entire region of the problem is divided into small discretized cubes of size $\delta \times \delta \times \delta$ (equal to the dimensions of the cubes forming the object), and Eq. (1) is discretized by the method of moments using roof-top functions as basis and testing functions. The resultant system of

#72603 - $15.00 USD Received 5 July 2006; revised 25 September 2006; accepted 30 September 2006

linear equations is then solved by iteration using a GMRES iteration with an FFT [13, 14].

The incident Gaussian beam, which propagates in the positive z direction, can be expressed as follows [15].

$$\boldsymbol{E}^{i}(\boldsymbol{x}) = E_0 W_0 / W(z) \exp[\,j\psi(z)]\{\boldsymbol{i}_x + \boldsymbol{i}_z\, j[1+\gamma^2(z)]^{-1/2}\gamma(z)\exp[\,j\psi(z)]\} \times \exp[-(x^2+y^2)/W^2(z)]\exp\{-jk_0(x^2+y^2)/[2R(z)]\}\exp(-jk_0 z), \tag{4}$$

where

$$W(z) = W_0[1+\gamma^2(z)]^{1/2},\quad \psi(z) = \tan^{-1}\gamma(z),\quad R(z) = z[1+1/\gamma^2(z)], \tag{5}$$

and

$$\gamma(z) = 2z/(k_0 W_0^{\,2}),\quad \gamma(x) = 2x/(k_0 W_0^{\,2}). \tag{6}$$

E_0 and W_0 are a constant amplitude and the beam waist (a half of the spot size) at $z = 0$, respectively. The validity of the code was checked by confirming that the code gives a reasonably accurate solution compared with the rigorous solution for a dielectric sphere and by confirming the energy conservation for a non-dissipative problem under a paraxial approximation.

The total far field $\boldsymbol{E}(r,\theta,\phi)$ of the spherical coordinates shown in Fig. 2 can be expressed as

$$\boldsymbol{E}(r,\theta,\phi) \approx [\exp(-jk_0 r)/(k_0 r)][\boldsymbol{F}^{\,s}(\theta,\varphi) + \boldsymbol{F}^{\,\mathrm{gauss}}(\theta,\varphi)] \tag{7}$$

where $\boldsymbol{F}^{s}(\theta,\phi)$ represents the scattered field generated by the aperture and the object, and is given by

$$\boldsymbol{F}^{\,s}(\theta,\varphi) = jk_0^3/(4\pi)\boldsymbol{i}_r \times \boldsymbol{i}_r \times \{\iiint_V [\varepsilon_r(\boldsymbol{x}') - 1]\boldsymbol{E}(\boldsymbol{x}')\exp(jk_0 \boldsymbol{x}'\cdot\boldsymbol{i}_r)\mathrm{d}v'\} \tag{8}$$

$\boldsymbol{F}^{\mathrm{gauss}}(\theta,\phi)$ represents the far field of the incident Gaussian beam and is given by

$$\boldsymbol{F}^{\,\mathrm{gauss}}(\pi,\phi) = F_\theta^{\,\mathrm{gauss}}(\theta,\phi)\boldsymbol{i}_\theta + F_\phi^{\,gauss}(\theta,\phi)\boldsymbol{i}_\phi \tag{9}$$

where

$$F_\theta^{\,\mathrm{gauss}}(\theta,\phi) = 2j(k_0 W_0/2)^2 E_0 \exp\{-[k_0 \sin\theta(W_0/2)]^2\}\cos\phi \tag{10}$$

$$F_\phi^{\,\mathrm{gauss}}(\pi,\phi) = 2j(k_0 W_0/2)^2 E_0 \exp\{-[k_0 \sin\theta(W_0/2)]^2\}\cos\theta\sin\phi \tag{11}$$

The total scattered power normalized by the incident power that can be observed in the conical region of $\theta_\alpha < \theta < \theta_\beta$ and $0 < \phi < 2\pi$ from the aperture can be expressed as

$$P(\theta_\alpha,\theta_\beta) = \int_{\theta_\alpha}^{\theta_\beta}\int_0^{2\pi} \left|\boldsymbol{F}^{\,s}(\theta,\phi) + \boldsymbol{F}^{\,\mathrm{gauss}}(\theta,\phi)\right|^2 \sin\theta\,\mathrm{d}\theta\,\mathrm{d}\phi/(\pi W_0^{\,2}/2) \tag{12}$$

The simulated image is generated by calculating the total scattered power according to Eq. (12).

#72603 - $15.00 USD Received 5 July 2006; revised 25 September 2006; accepted 30 September 2006

4. Simulated optical images

In the simulation, the wavelength (λ) is set at 573 nm, and the relative permittivities of the metallic screen, the dielectric object and the surrounding free space are fixed at $\varepsilon_r(\boldsymbol{x})/\varepsilon_0 = \varepsilon_1 = -12.4 - j0.85$ (silver), $\varepsilon_r(\boldsymbol{x})/\varepsilon_0 = \varepsilon_2 = 2.25$ (glass), and $\varepsilon_r(\boldsymbol{x})/\varepsilon_0 = 1.0$, respectively. The parameters of the incident wave are $E_0 = 1$ and $W_0 = \lambda$. The electric incident vector $E^i(\boldsymbol{x})$ at $z = 0$ is fixed parallel to the x axis in Fig. 1. All lengths are normalized with respect to the wavenumber $k_0 = 2\pi/\lambda$. The screen thickness is given by $k_0 w = 1.4$ (approximately 0.22λ, 128 nm) with a tip-probe height of $k_0 h = 0.5$ (approximately 0.08λ, 46 nm). The height difference between the two pyramidal sections is given by $k_0 g = 0.4$ (0.06λ, 36 nm). For the I-shaped aperture, $k_0 a_x = 0.5$, $k_0 a_y = 0.4$, $k_0 b_x = 1.0$ (0.16λ, 91 nm) and $k_0 b_y = 1.8$ (0.29λ, 164 nm) are fixed. The size of the screen used in the numerical evaluation is $k_0 C_x = k_0 C_y = 21.2$ (3.4λ, 1933 nm), and the size of discretized cubes is $k_0\delta = 0.1$ (0.016λ, 9 nm).

We show a part of the cross section of the screen and pyramidal structure that contains probe tip which consists of one descretized cube whose size is given by $k_0\delta \times k_0\delta \times k_0\delta = 0.1 \times 0.1 \times 0.1$ on the plane parallel to the x-z plane and to the y-z plane in Figs. 3(a) and 3(b), respectively.

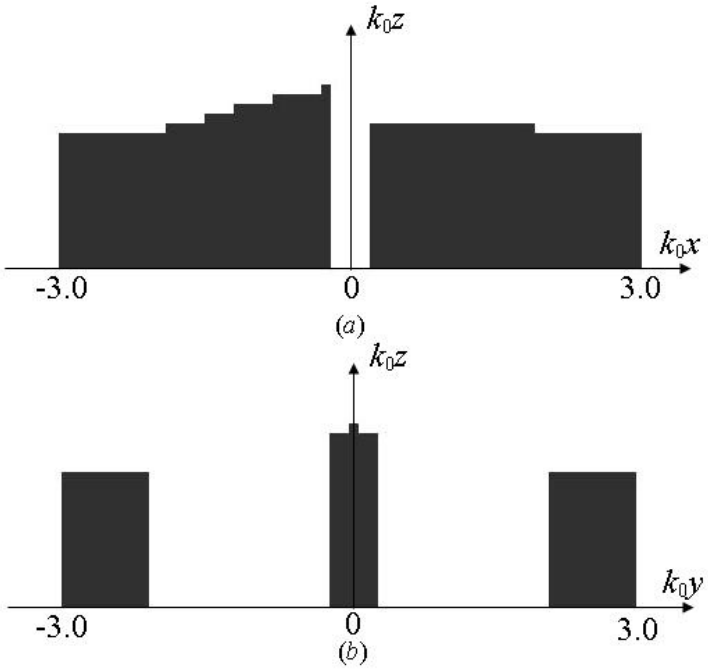

Fig. 3. Cross section of the screen and pyramidal structure that contains probe tip which consists of one descretized cube of size on the plane parallel (a) to the x-z plane in the range $-3.0 < k_0x < 3.0$ only and (b) to the y-z plane in the range $-3.0 < k_0y < 3.0$ only.

For a PGP tip prepared at the end of an optical fiber, simulated images can be obtained in illumination and collection-reflection modes by calculating the ranges $P(0,\pi/2)$ and $P(\pi/2,\pi)$ in Eq. (12), respectively. If the direction of the incident Gaussian beam is reversed, that is, incidence is from the positive z direction in Fig. 1, the result for collection mode can be obtained by calculating $P(\pi/2,\pi)$ in Eq. (12).

Simulations of the total scattered power were conducted for the probe tip positioned at

#72603 - $15.00 USD Received 5 July 2006; revised 25 September 2006; accepted 30 September 2006

each of 9×9 grid points (δ apart) on the plane parallel to the object plane. The image obtained reflects the dependence of the calculated scattered power on the position of the probe tip. The scanning probe is assumed to be held in close proximity to the object surface, that is, $k_0 d = 0$ (Fig. 1). The system used in the simulations is a cluster of nine 1.6 GHz Pentium IV processors running Linux with 2GB memory on each node. The maximum computational time to complete 9×9 pixels was about 100 hours and the maximum used memory was 1.8GB on each node.

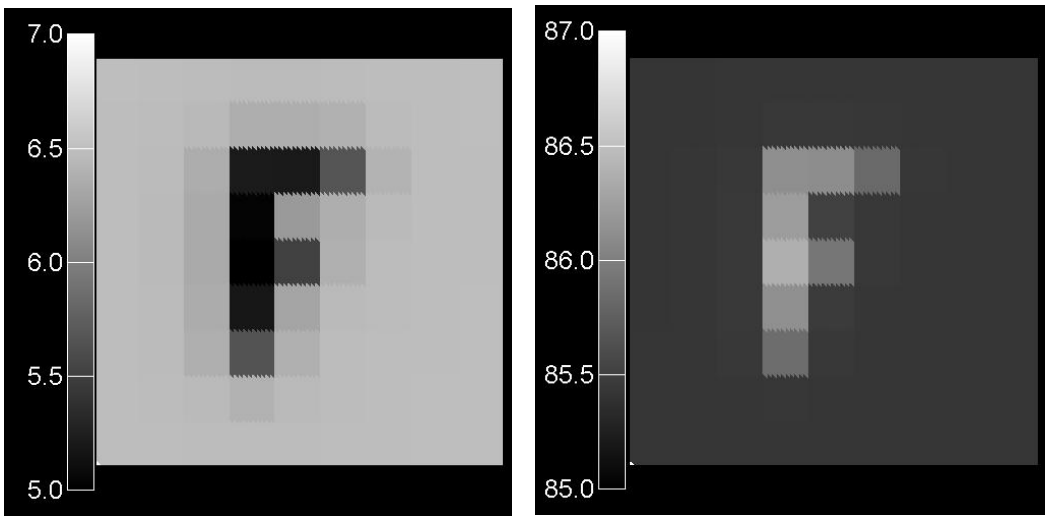

(a) (b)

Fig. 4. Simulated image of F-shaped dielectric object for (a) illumination mode with $P(0,\pi/2)$, and (b) collection-reflection mode with $P(\pi/2,\pi)$. Grayscale represents the percentage of incident power determined by Eq. (12) (range is 2% of incident power).

The tip of the left pyramidal section (i.e., the probe tip) is modeled as a single discretized cube with side length $k_0\delta$ (=0.1) shown in Fig. 3 [2]. The grayscale image for the illumination-mode scan is shown in Fig. 4(a). In this case, the average throughput of the aperture was approximately 6.3% of the incident power and the image contrast (the deference between maximum and minimum values of pixels) was 1.7% of the incident power. In the conventional aperture probe, the experimental throughput is ranging from 10^{-2} to 10^{-5} for a 100 nm – 40 nm aperture diameter (λ=400 nm) in the references [16, 17] and from 10^{-5} to 10^{-9} for a 90 nm – 20 nm aperture diameter (λ=632.5 nm) in the reference [18]. We can consider that the resolution of the conventional aperture probe is approximately similar to the aperture diameter. Since the throughput depends on the spot size of the Gaussian beam used in our calculation, it is not reasonable to compare our results with above experimental results directly. However, the throughput shown in Fig. 4(a) shows the extremely high throughput compared to a conventional aperture probe, whose diameter is smaller than 100 nm, giving a similar resolution. This large throughput is due to the fact that the aperture of PGP is sufficiently long to avoid the cutoff condition.

In this example, the signal corresponding to the locations of cubes forming the F-shaped object is weaker than the background. In collection-reflection mode [Fig. 4(b)], the average reflected power is approximately 85.5% and the image contrast is 0.9% of the incident power, affording a higher signal over the object compared to the background. The resolution in these

#72603 - $15.00 USD Received 5 July 2006; revised 25 September 2006; accepted 30 September 2006

two cases is approximately equal to the tip diameter (9 nm), indicating that the resolution of the PGP as implemented in Fig. 1 is determined by the tip diameter. Previous studies have shown that the scattering probe can achieve a resolution equal to the probe radius [3–7]. However, those results have been obtained under the assumption that the probe is an isolated sphere. The present results, obtained without such an assumption, show that the PGP acts as an isolated sphere probe under practical conditions.

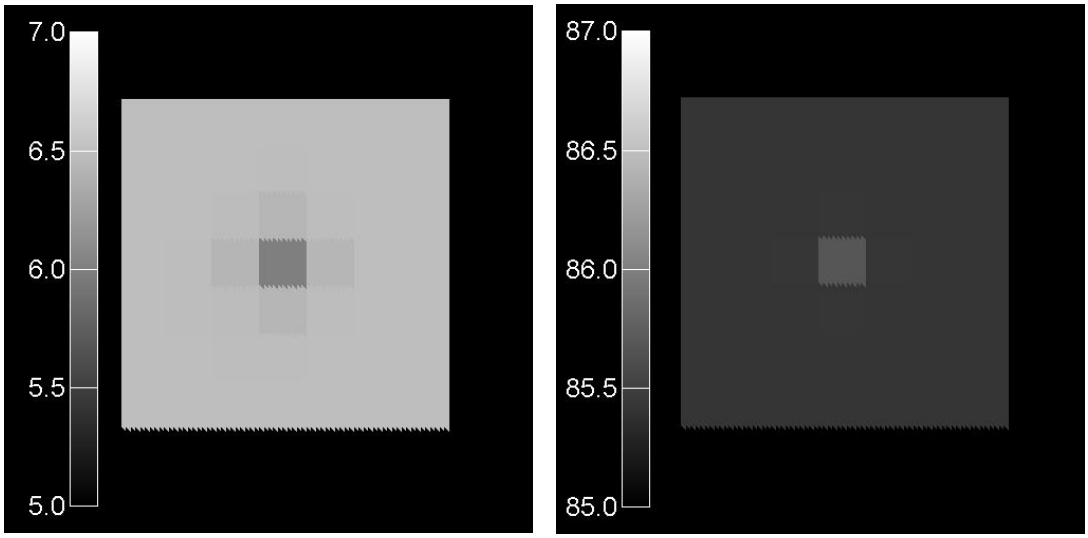

(a) (b)

Fig. 5. Simulated image of single isolated dielectric object. (a) illumination mode with $P(0,\pi/2)$, and (b) collection-reflection with $P(\pi/2,\pi)$. Grayscale represents the percent of incident power determined by Eq. (12).

Simulated images for a single dielectric cube, whose size is given by $\delta \times \delta \times \delta$, in a 7×7 pixel plane are shown in Figs. 5(a) and 5(b) for illumination mode and collection-reflection mode. The contrast in Fig. 5 for a single dielectric cube is similar to that in Fig. 4 for the F-shaped object. These results indicate that the localized and enhanced near field created at the tip of the PGP interacts with the dielectric object only in the range limited by the tip diameter. It is therefore reasonable to conclude that the resolution in the resultant scanning image corresponds to the tip diameter. This characteristic makes the PGP ideal as a scanning probe for NSOM.

The basic imaging characteristics by the probe can be explained by the simple dipole-dipole interaction theory [19, 20]. By approximate the probe and object by dielectric spheres with small diameter, we can simply calculate the spatial resolution and image contrast. In this theory, the resolution of the probe tip is approximately to equal to the diameter of the probe tip and optimal contrast can be obtained when diameter of the probe sphere is similar to the object sphere. Our simulation results are not contradicted with the dipole-dipole interaction theory.

#72603 - $15.00 USD Received 5 July 2006; revised 25 September 2006; accepted 30 September 2006

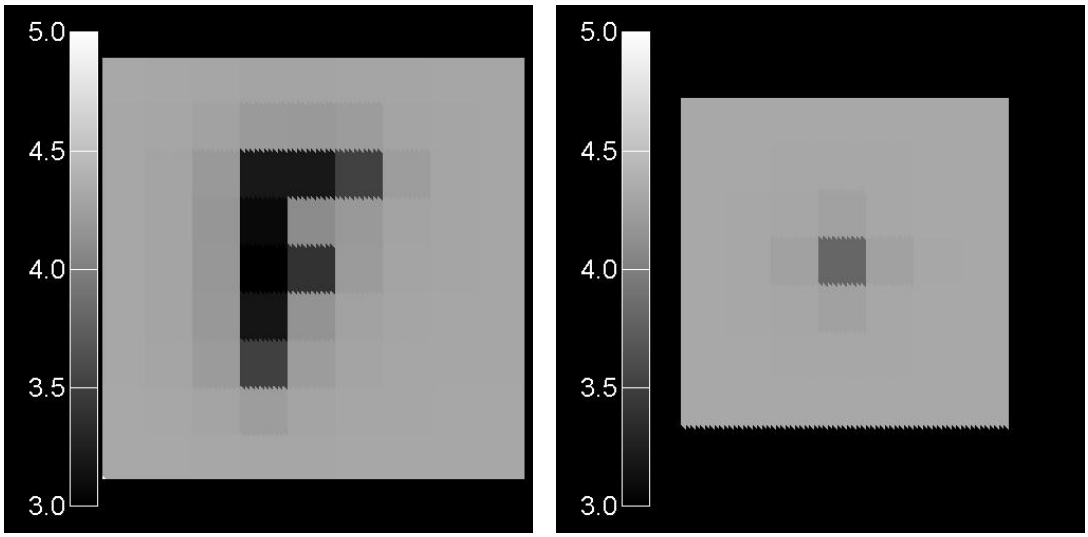

(a) (b)

Fig. 6. Simulated images of collection-mode scan with $P(\pi/2,\pi)$ for a wave incident from the positive z direction (see Fig. 2). (a). Image of F-shaped dielectric object in a 9×9 pixel plane. (b). Image for a single dielectric cube in a 7×7 pixel plane.

The results for collection mode are shown in Fig. 6. The average throughput of the aperture in this mode was approximately 4.2%, and the image contrast was 1.4% of the incident power in Fig. 6(a). It is considered that conventional scattering probes can be used in illumination mode only, since the signal is measured from the scattering waves at the tip and not by collection [21], [22]. It is thus very interesting that the proposed PGP works in both collection-reflection mode and collection mode yet has the resolution of a scattering probe (i.e., corresponding to the tip diameter).

To confirm the results above, further simulations were conducted for a larger tip diameter and a larger distance d between the tip and the object surface. The probe tip in this case was modeled as a rectangular parallelepiped consisting of $2 \times 2 \times 1$ discretized cubes [2], giving a probe tip of larger radius than in the previous examples. The results are shown in Fig. 7(a) for $k_0 d = 0$. In this case, the average throughput was 6.4%, and the average contrast was 0.3% of the incident power. Figure 7(b) shows the result of increasing the distance between the tip and the object surface to $k_0 d = 0.1$. The tip is modeled as a single discretized cube with side length $k_0\delta$ in this case. The average throughput in this case was 6.5% and the average contrast was 0.04% of the incident power. The resolution and contrast are considerably degraded in both cases, in agreement with dipole-dipole interaction theory [19, 20].

#72603 - $15.00 USD Received 5 July 2006; revised 25 September 2006; accepted 30 September 2006

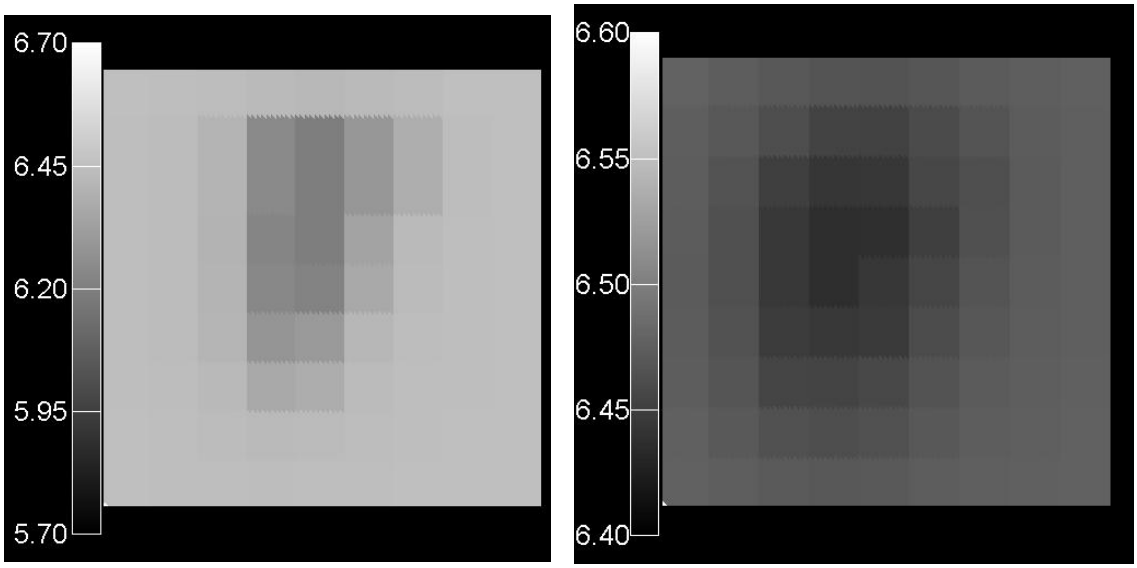

(a) (b)

Fig. 7. Simulated images of illumination mode scan with $P(0, \pi/2)$. (a) Probe tip consists of $2 \times 2 \times 1$ discretized cubes. Distance between object plane and probe tip is $k_0 d = 0$. (b) Distance between object plane and probe tip is $k_0 d = 0.1$. Probe tip consists of one discretized cubes.

5. Effects of the substrate

We have considered the imaging of the nanometric F-shaped dielectric object which is placed in the free space shown in Figs. 1 and 2. In the practical situation, the object must be placed on the substrate. In order to investigate the effects of the substrate, we placed the dielectric slab (rectangular parallelepiped) on the F-shaped object in Figs. 1 and 2. The size of the slab is given by $k_0 C_x \times k_0 C_y \times k_0 w_{slab} = 21.2 \times 21.2$

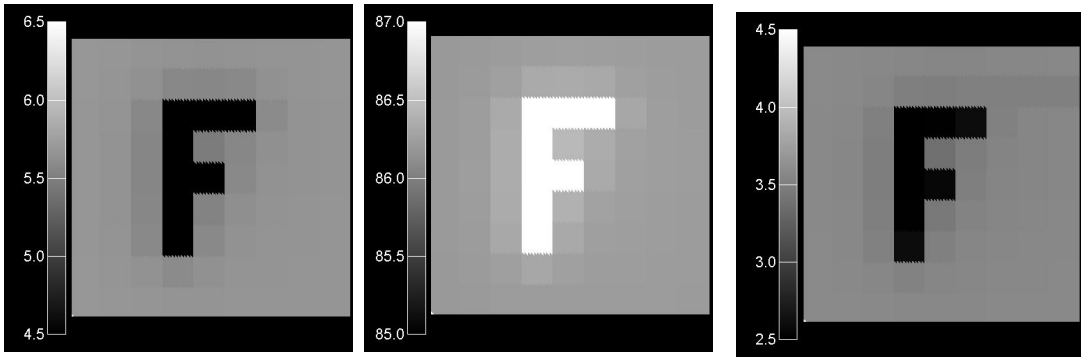

(a) (b) (c)

Fig. 8. Simulated images of the object with the substrate of (a) illumination-mode scan with $P(0, \pi/2)$, (b) collection-reflection mode scan with $P(\pi/2,\pi)$ and (c) collection mode scan with $P(\pi/2,\pi)$.

#72603 - $15.00 USD Received 5 July 2006; revised 25 September 2006; accepted 30 September 2006

$\times 0.6$, where w_{slab} is the thickness of the slab. The relative permittivity of the slab is given by $\varepsilon_3 = 2.25$. The simulation results for the case of $k_0 d = 0$ with constant height scanning are shown in Fig. 8(a)-8(c) for illumination mode, collection-reflection mode, and collection mode, respectively. Basic image characteristics are very similar to the results without substrate. Since we have found that the localized near field at the tip of the PGP interacts with the object only in the range limited by the tip diameter, it is reasonable that the effects of the substrate is minor. Because, the distance between tip and substrate surface is larger than that between tip and object surface in the constant height scanning.

6. Conclusion

Simulations of image acquisition were performed for near-field scanning optical microscopy (NSOM) with a plasmonic gap probe (PGP). The PGP works in illumination, collection-reflection and collection mode, and it is not necessary to vibrate the probe tip in order to remove the background noise. It was demonstrated that the resolution of the images approximately corresponds to the probe-tip diameter. The PGP thus offers the advantages of both aperture probes and scattering probes. Furthermore, the throughput of the probe is extremely high compared to conventional aperture probes giving similar resolution. The simulation results obtained in this study confirm that the proposed PGP probe should have excellent characteristics as a scanning probe for NSOM.

The quantitative results of the simulated images are strongly dependent on the parameters of the probe structure. For example, throughput, contrast, and the brightness variation in the simulated image depend on the shape of the I-shaped aperture. These image characteristics in detail are currently under further investigation. However, basic qualitative characteristics of PGP, i.e., high resolution and large throughput and availability of collection mode, are not strongly dependant on these parameters in our simulation.

Acknowledgments

The authors thank to Tatsuhiko Sugiyama for help in the numerical evaluations. This research was partially supported by the Ministry of Education, Science, Sports and Culture, Grant-in-Aid for (C), 18560034, 2006.

#72603 - $15.00 USD Received 5 July 2006; revised 25 September 2006; accepted 30 September 2006